Biomedical Signal Processing and Control 52 (2019) 111–119

Contents lists available at ScienceDirect

Biomedical Signal Processing and Control

journal homepage: www.elsevier.com/locate/bspc

Multi-lead ECG signal analysis for myocardial infarction detection and localization through the mapping of Grassmannian and Euclidean features into a common Hilbert space

Panagiotis Barmpoutis [a], Kosmas Dimitropoulos [b], Anestis Apostolidis [c], Nikos Grammalidis [b,*]

[a] Department of Electrical and Electronic Engineering, Faculty of Engineering, Imperial College London, SW7 2AZ, United Kingdom
[b] Visual Computing Lab., Information Technologies Institute, Center for Research and Technology Hellas, 57001, Greece
[c] Department of Electrical and Computer Engineering, Faculty of Engineering, Aristotle University, Hellas, 54124, Greece

ARTICLE INFO

Article history:
Received 19 November 2018
Received in revised form 19 March 2019
Accepted 6 April 2019
Available online 15 April 2019

Keywords:
Electrocardiograms
Myocardial infraction
Linear dynamical systems
Reproducing Kernel Hilbert space

ABSTRACT

Background and objective: Electrocardiogram is commonly used as a diagnostic tool for the monitoring of cardiac health and the detection of possible heart diseases. However, the procedure followed for the diagnosis of heart abnormalities is time consuming and prone to human errors. Thus, the development of computer-aided techniques for the automatic analysis of electrocardiogram signals is of vital importance for the diagnosis and prevention of heart diseases. The most serious outcome of coronary heart disease is the myocardial infarction, i.e., the rapid and irreversible damage of cardiac muscles, which, if not diagnosed and treated in time, continues to damage further the myocardial structure and function. In this paper we propose a novel approach for the automatic detection and localization of myocardial infarction from multi-lead electrocardiogram signals.
Methods: The proposed method initially reshapes the multidimensional signal into a third-order tensor structure and subsequently extracts feature representations in both Euclidean and Grassmannian space. In addition, two different methods are proposed for the mapping of the two different feature representations into a common Hilbert space before the final classification of signals. The first approach is based on the mapping of both Grassmannian and Euclidean features in a Reproducing Kernel Hilbert Space (RKHS), while the second one attempts to initially apply Vector of Locally Aggregated Descriptors (VLAD) encoding directly to Grassmann manifold and then concatenate the two VLAD representations.
Results: For the evaluation of the proposed method, we have conducted extensive tests using a publicly available dataset, namely PTB Diagnostic ECG database, containing 549 multi-lead ECG data recordings from 290 subjects and from different diagnostic classes. The method provides an excellent detection rate of 100%, and localization rate, i.e., 100% with the first fusion method and 99.7% with the second one.
Conclusions: The Experimental results presented in this paper show the superiority of the proposed methodology against a number of state-of-the-art approaches. The main advantage of the proposed approach is that it exploits better the intercorrelations between signals of different ECG leads, by extracting feature representations that lie in different geometrical spaces and contain complementary information with regard to the dynamics of signals.

1. Introduction

Cardiovascular diseases (CVDs) are related to a number of factors preventing the flow of blood to heart or brain and are considered as the number one cause of death globally [1]. In severe conditions, deaths are due to the occlusion of the coronary artery caused by the rupturing of atherosclerotic plaques [2], something that constitutes the main pathogenesis for the majority of Myocardial Infarctions (MI). More specifically, the MI is one of the five main manifestations of coronary heart disease [1] and occurs when the blood flow decreases or stops to a part of the heart, causing damage to the heart muscle. Myocardial infarction can be recognized by clinical symptoms and features, including elevated values of

* Corresponding author.
E-mail addresses: p.barmpoutis@imperial.ac.uk (P. Barmpoutis), dimitrop@iti.gr (K. Dimitropoulos), anestapostol@gmail.com (A. Apostolidis), ngramm@iti.gr (N. Grammalidis).

https://doi.org/10.1016/j.bspc.2019.04.003
1746-8094/

biochemical markers (biomarkers) of myocardial necrosis and by imaging [3].

Recent advances in digital diagnostic technology can contribute significantly to the detection of even minor MI events of cardiac patients effectively. Towards this direction, electrocardiogram (ECG) is an important tool for doctors, providing vital information with regard to the function and rhythm of human heart [4]. ECG signals are used for the diagnosis of cardiac symptoms and the detection of a variety of heart diseases like myocardial infarction (MI), cardiac dysrhythmias and pulmonary embolism. More specifically, MI produces changes in the ECG signal appearing T waves abnormally high, longer than normal QT intervals and abnormal elevation of ST segment [5]. As the nature and amplitude of P, Q, R, S, T waves in the ECG signals changes depending on the lead, the use of multiple ECG leads is required for an accurate analysis. Different types of MI can be observed in specific leads depending on the location of infarction in the myocardium.

Nowadays, to overcome time and reliable limitations of manual analysis of ECGs, several computer-aided signal processing methods have been proposed in order to detect and localize MI from ECG signals [6]. As ECG signals can be corrupted by unwanted interferences (e.g., power line interference, electrode contact noise, instrumentation noise, etc.), an important preprocessing step before their analysis is the signals denoising procedure. For this reason, several approaches have been proposed aiming to denoise ECG signals, facilitating their accurate interpretation. More precisely, for this purpose, combinations of empirical mode decomposition and variational mode decomposition with discrete wavelet transform [7] and constrained least squares optimization have been used [8,9]. More recently, Padhy and Dandapat [10] employed a high-pass filter and a "Zero-phase forward and reverse digital filter" in order to remove baseline-wander. Then, to accurately extract features from biomedical and ECG signals, many researchers have used discrete wavelet transform (DWT) techniques [11–13], as DWT has been proved an efficient tool for the analysis of this kind of signals. More specifically, Zhao and Zhang [14] proposed the use of wavelet transform and support vector machines, while for the estimation of subtle changes of ECG signals, Jayachandran [15] utilized the multiresolution properties of DWT to identify characteristic points in ECG signal and computed the entropy in the wavelet domain. On the other hand, other researchers [16] have proposed the use of Fourier harmonic phases of the ECG data, which is advantageous in terms of computational simplicity.

However, the majority of the aforementioned techniques is based on the analysis of single-lead ECGs instead of multi-lead ECG (MECG) signals. In [17], the authors presented an automatic detection and localization approach of myocardial infarction (MI) using K-nearest neighbor (KNN) classifier. Specifically, time domain features of each beat in the ECG signal, which are indicative of MI, such as T wave amplitude, Q wave and ST level deviation are extracted from 12 leads ECG. In another research work, Sharma, et al. introduced a novel technique based on a multiscale energy and eigenspace (MEES) approach for the detection and localization of MI [18]. Furthermore, Padhy and Dandapat proposed a method for MI detection and localization where higher-order singular value decomposition was applied to a third-order MECG tensor for dimensionality reduction [19], while for the detection and localization of MI a multi-class SVM classifier was used.

Recently, deep learning networks have been employed in the automated classification of ECG signals and detection of numerous heart diseases [20,21]. For MI detection, Acharya et al. [5], used a 11-layer deep CNN algorithm for the detection of MI using ECG multi-lead signals with and without noise. Furthermore, Liu et al. [22], used a deep convolution neural network (CNN) using electrocardiogram (ECG) signal from the lead II and taking 3-s signal segments as input. Although these methods do not rely on the extraction of handcrafted features, the training of complex deep learning networks requires the creation of large datasets for the accurate definition of their parameters.

Inspired by the analysis of multidimensional evolving signals through DWT and Linear Dynamical Systems (LDS), in this paper, we propose a novel approach for MI detection and localization that exploits better the inter-correlations between signals of different ECG leads by extracting feature representations that lie in different geometrical spaces and contain complementary information with regard to the dynamics of signals. LDSs have been successfully used in the past in a broad range of applications in engineering (e.g., dynamic texture analysis [23], human action recognition [24], and grading of invasive breast carcinoma [25]), however to the best of our knowledge this is the first time that higher-order LDSs are used for the modeling of multi-lead ECG signals. In addition, we propose two different fusion approaches for mapping the extracted feature representations into a common Hilbert space. The proposed approaches can also be applied to other application fields, in which the fusion of feature representations that belong to different geometrical subspaces is required. More specifically, the contributions of this work can be summarized in the following aspects:

- We introduce a novel methodology for automated myocardial infarction detection and localization, aiming to improve classification accuracy by fusing different feature representations with complementary information into a common Hilbert space. The proposed methodology has been benchmarked in a popular publicly available dataset with favorable results.
- In order to exploit the hidden beat and lead correlations, we propose the modeling of multi-lead ECG signals through a higher-order LDS and the projection of LDS parameters to a Grassmann manifold.
- Moreover, we extract feature representations in the Euclidean space by encoding multi-lead ECG signals as VLAD representations after a dyadic discrete wavelet transform and a subsequent multiscale higher-order SVD analysis on sub-band tensors.
- Finally, we propose two fusion approaches for mapping the extracted feature representations in a common Hilbert space. The first approach is based on the mapping of both Grassmannian and Euclidean features in a Reproducing Kernel Hilbert Space (RKHS), while the second one attempts to apply VLAD encoding directly to Grassmann manifold and then concatenate the two VLAD representations. Both approaches are generic and can be easily applied to various application fields.

The remainder of this paper is organized as follows: Section 2 presents the proposed methodology including data preprocessing, ECG signals modeling, fusion of feature representations and classification. Subsequently, the dataset and experimental results are discussed in Section 3, while finally conclusions are drawn in Section 4.

2. Methods

The overall structure of the proposed methodology for the classification and localization of MI is shown in Fig. 1. More specifically, multi-lead ECG signals are initially pre-processed and reshaped into a third-order tensor structure. Subsequently, for the modeling of the third-order tensor representation of data, we apply: i) a higher-order LDS modelling in order to extract the dynamics of the multi-lead signal and ii) a dyadic discrete wavelet transform followed by a multiscale higher-order SVD analysis on sub-band tensors to exploit the intra-beat, inter-beat and inter-lead correlations. In the first case, LDS descriptors are mapped into a Grassmann manifold, while in the second one VLAD encoding is applied. Finally,

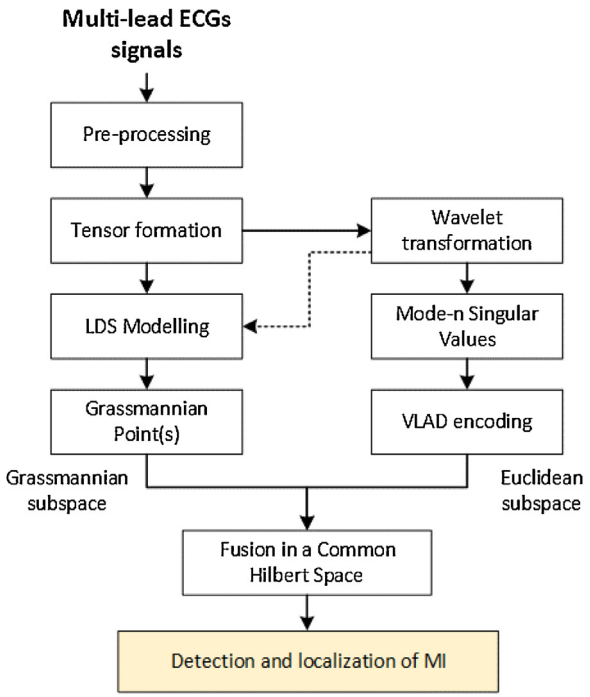

Fig. 1. The proposed methodology.

both Euclidean (VLAD encodings) and Grassmannian feature representations are mapped and fused in a common Hilbert space for the detection and localization of MI. We have to note here that alternatively, we can also model the sub-band tensors of wavelet transform using higher-order linear dynamical systems to create multiple Grassmannian subspaces. This issue is discussed in detail in Section 2.4.2.

2.1. Data preprocessing and tensor ECG formation

In this first preprocessing step, we attempt to bring the leads of ECG to their isoelectric levels by passing each ECG signal through a digital Butterworth high-pass filter with a cut-off frequency of 0.5 Hz, and a "Zero-phase forward and reverse digital filter", as proposed in [10]. Additionally, R-peak detection and period normalization is performed, while subsequently each lead signal is segmented and normalized to the number of beat periods. After the preprocessing of the recorded signals, the multi-lead ECG data is reshaped into a third-order tensor structure. More specifically, this data is represented as $Y \in \mathbb{R}^{l\times b\times s}$, where the dimensions l, b, and s are respectively the number of leads, heart beats, and consecutive samples of normalized heartbeat. The horizontal slices of Y represent each ECG lead, and each vector of a horizontal slice represents consecutive beats of a lead [19].

2.2. Mapping of ECGs signals into Grassmann manifold

The output of an ECG signal indicates the electrical activity generated by the heart as a function of time and it is a near-periodic signal for a specific time. In a multi-lead ECG the leads refer to imaginary lines between two ECG electrodes. To exploit this information, in this paper we attempt to model the interdependent 12-lead signals and beats of ECGs using LDSs. A linear dynamical system is associated with a first order ARMA process with white zero mean IID Gaussian input and for this reason LDSs are also known as linear Gaussian state-space models. In general, LDS models attempt to associate the output of the system, i.e., the observation, with a linear function of a state variable, while in each time instant, the state variable depends linearly on the state of the previous time instant. Both state and output noise are zero-mean normally distributed random variables and apart from the output of the system, all other variables (state and noise variables) are hidden. The adopted system is described by the following equations:

$$x(t+1) = Ax(t) + Bv(t) \tag{1}$$

$$y(t) = \bar{y} + Cx(t) + w(t) \tag{2}$$

where $x \in R^n$ is the hidden state process, $y \in \mathbb{R}^d$ is the observed data, $A \in \mathbb{R}^{n\times n}$ is the transition matrix of the hidden state and $C \in \mathbb{R}^{d\times n}$ is the mapping matrix of the hidden state to the output of the system. The quantities $w(t)$ and $Bv(t)$ are the measurement and process noise respectively, with $w(t)\tilde{N}(O, R)$ and $Bv(t)\tilde{N}(0, Q)$, while $\bar{y} \in \mathbb{R}^d$ is the mean value of the observation data. The extracted tuple LDS descriptor, $M = (A, C)$, models both the appearance and dynamics of the observation data, represented by C and A, respectively. The descriptor's parameters, A and C, can be estimated through a suboptimal method initially proposed by Doretto et. al [26].

However, in our case the multi-lead ECG signal is represented by the third-order tensor Y. To this end, we decompose the ECG formation Y using a higher order singular value decomposition:

$$Y = S \times_1 U^{(1)} \times_2 U^{(2)} \times_3 U^{(3)} \tag{3}$$

where $S \in \mathbb{R}^{l\times b\times s}$ is the core tensor, while $U^{(1)} \in \mathbb{R}^{l\times l}$, $U^{(2)} \in \mathbb{R}^{b\times b}$ and $U^{(3)} \in \mathbb{R}^{s\times s}$ are orthogonal matrices containing the orthonormal vectors spanning the column space of the matrix and $\times_j$ denotes the j -mode product between a tensor and a matrix. Since the columns of the mapping matrix C of the stochastic process need to be orthonormal, we can consider $C = U^{(3)}$ and

$$X = S \times_1 U^{(1)} \times_2 U^{(2)} \tag{4}$$

Then, the transition matrix A can be estimated using least squares [27] as follows:

$$A = X_2 X_1^T (X_1 X_1^T)^{-1} \tag{5}$$

where $X_1 = [x(2), x(3), \ldots, x(t)]$ and $X_2 = [x(1), x(2), \ldots, x(t-1)]$.

Furthermore, to improve the stability of the dynamical system (i.e., to estimate the stabilized transition matrix A), we obtain an approximate solution, based on a convex optimization technique [28], by solving the following quadratic problem:

$$\text{minimize } aPa - 2q^T a + r \tag{6}$$

$$\text{subject to } g^T a \leq 1 \tag{7}$$

where $a = vec(A)$, $q = vec(X_1 X_2^T)$, $r = tr(X_2^T X_2)$ and $P = I \otimes (X_1^T X_1)$, I is the identity matrix, $tr(\cdot)$ indicates the trace of a matrix and $vec(\cdot)$ operator converts a matrix to vector and $\otimes$ denotes the Kronecker product. Also, $g = vec(u_1 v_1^T)$ where vectors u_1 and v_1^T correspond to the first eigenvalue of the transition matrix A.

Having modeled each ECG signal using a higher-order linear dynamical system approach, our next step is to represent the parameters of each dynamical system, $M = (A, C)$, as a point on the space of the extracted descriptors. Towards this end, we initially estimate the finite observability matrix of each dynamical system, $O_m^T(M) = \left[C^T, (CA)^T, \left(CA^2\right)^T, \ldots, \left(CA^{m-1}\right)^T\right]$ and then, we apply a Gram-Schmidt othonormalization [29] procedure, i.e., $O_m^T = GR$, in order to represent each descriptor M as a point, $G \in \mathbb{R}^{m\times T\times 3}$, on the Grassmann manifold (in our experiments we set the size m of the observability matrix equal to 3, while T is the number of samples).

2.3. Modelling of ECG signal using locally aggregated descriptors

In this section, we propose the representation of ECG signals, i.e., the third-order tensor Y, as a VLAD. The extracted VLAD descriptor can be considered intrinsically as Euclidean, as it encodes the features' distribution in their native vector space. More specifically, we initially apply a dyadic discrete Wavelet Transform (with Daubechies 9/7 Biorthogonal wavelet filters as mother wavelet) on every vector $Y(i,j,:)$ of the tensor $Y \in \mathbb{R}^{l\times b\times s}$ where $i=1,\ldots,l$ and $j=1,\ldots,b$. This transformation results $2\times L$ sub-band tensors (L is the number of levels and depends on the sampling frequency of the signal) comprising of one approximation $A_L \in r^{l\times b\times s_A}$, with $s_A = s/2\hat{L}$, and L number of details D_k (where $k=1,\ldots,L$) sub-band tensors with dimensions $l\times b\times s_k$, with $s_k = s/2\hat{k}$ [19]. Subsequently, each sub-band tensor is decomposed according to Eq. (3) and a feature vector is formed by the concatenation of mode- n singular values σ (in our case n is equal to 3) of all extracted core tensors S. In particular, for the 3 modes of each sub-band tensor A_L and D_k, we form the corresponding feature vectors:

$$x_L^A = \left[\sigma_1^{(1)},\ldots,\sigma_l^{(1)},\sigma_1^{(2)},\ldots,\sigma_b^{(2)},\ldots,\sigma_1^{(3)},\ldots,\sigma_{s_A}^{(3)}\right] \tag{8}$$

and

$$y_k^D = \left[\hat{\sigma}_1^{(1)},\ldots\hat{\sigma}_1^{(1)},\hat{\sigma}_1^{(2)},\ldots\hat{\sigma}_b^{(2)}\ldots,\hat{\sigma}_1^{(3)},\ldots\hat{\sigma}_{s_k}^{(3)}\right] \tag{9}$$

and then, we concatenate the individual features to form the final feature vector as follows:

$$v = [x_L^A, y_{L,}^D, y_{L-1}^D,\ldots,y_1^D] \tag{10}$$

In our experiments we extracted the singular values of sub-band tensors A_7, D_7, D_6, D_5 and D_4 and used the first three singular values of each unfolded submatrix for the construction of feature vectors in Eqs. (8) and (9). These sub-bands contain 'PQRST' segmented information, while the rest do not contain any meaningful information [19].

Finally, for the modelling of each ECG signal, we apply VLAD encoding, which is considered as a simplified coding scheme of the earlier Fisher Vector (FV) representation and has shown to outperform histogram representations in bag of features approaches [30,31]. More specifically, we consider a codebook, $\{m_i\}_{i=1}^r = \{m_1, m_2,\ldots,m_r\}$, with r visual words and local descriptors v, where each descriptor is associated to its nearest codeword $m_i = NN(v_j)$. The VLAD descriptor, V, is created by concatenating the r local difference vectors $\{u_i\}_{i=1}^r$ corresponding to differences $v_j - m_i$, with $m_i = NN(v_j)$, where v_j are the descriptors associated with codeword i, with $i=1,\ldots,r$.

$$\overline{V} = \{u_i\}_{i=1}^r = \{u_1,\ldots,u_r\} \tag{11}$$

or

$$\bar{V} = \left\{ \sum_{\substack{v_j \text{ such that}\\ m_1 = NN(v_j)}} (v_j - m_1), \ldots, \sum_{\substack{v_j \text{ such that}\\ m_r = NN(v_j)}} (v_j - m_r) \right\} \tag{12}$$

while the final VLAD representation is determined by the L2-normalization of vector $\bar{V}$:

$$\overline{V}_{Euclidean} = \overline{V}/\left\|\overline{V}\right\|_2 \tag{13}$$

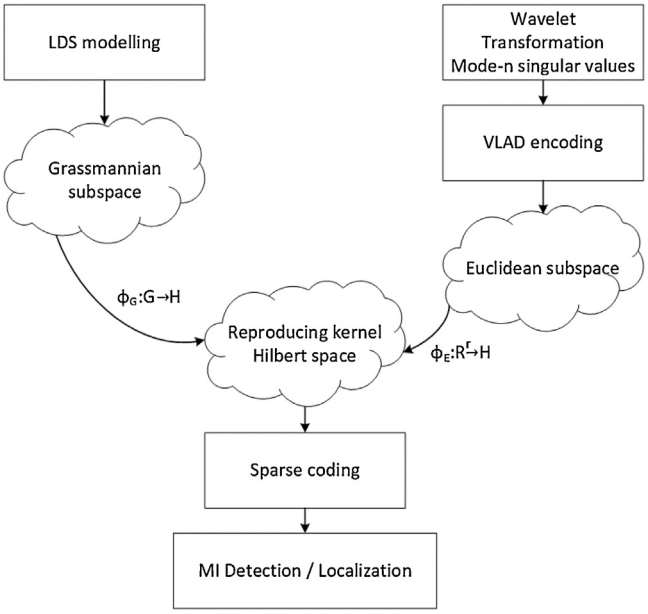

Fig. 2. Proposed-1 fusion approach using different kernel functions for mapping Grassmannian and Euclidean data into a common Hilbert space.

2.4. Fusion of feature representations in a common space

2.4.1. Fusion through the mapping of data in a reproducing Kernel Hilbert Space

To fuse the extracted feature representations, we propose in this section their mapping into a common Hilbert space H (it is defined as *proposed-1*). Our main problem here stems from the fact that the two feature representations, i.e., Grassmannian points and VLAD encodings, lie in different geometrical spaces. More specifically, in the first case we have points in the non-Euclidean space of the dynamical model, known as Grassmann manifold, which is a quotient of the special orthogonal group $SO(n)$, i.e., the subset of all orthogonal matrices with determinant equal to +1 (this simply means that we can extend the notion of tangent spaces, geodesics etc. from the base manifold $SO(n)$ to the quotient space of Grassmann manifold). On the other hand, the second feature representation is a VLAD descriptor, which lies in Euclidean space (Fig. 2).

To address the problem, we attempt to transform the two feature representations into a common Hilbert space using two kernel functions, $\varphi_G : G\to H$ for the Grassmann manifold and $\varphi_E : \mathbb{R}^r\to H$ for the Euclidean space. In the first case, the Grassmannian kernel $k_G(g_1,g_2)$, which shows the similarity between two Grassmannian points g_1 and g_2 is estimated using the inverse exponential map on the Grassmann manifold:

$$k_G(g_1,g_2) = d_G(g_1,g_2) = \left\|exp_{g_2}^{-1} g_1\right\|_F \tag{14}$$

where $\|\cdot\|_F$ is the matrix Frobenius norm. For estimating the inverse exponential map, we first need to compute the orthogonal completion O_r of g_1 and then the thin CS decomposition of matrix $O_r^T g_2$ to find the direction matrix that specifies the direction and speed of geodesic flow [24]. On the other hand, for the Euclidean space, we can simply apply a Radial Basis Function (RBF) kernel for two feature vectors x_1 and x_2:

$$k_E(x_1,x_2) = exp\left(-\frac{\|x_1 - x_2\|^2}{2\sigma^2}\right) \tag{15}$$

Using Eqs. (14) and (15) as similarity metrics in Grassmannian and Euclidean space respectively, we can easily estimate the elements

of kernel matrices K_G and K_E. To improve the robustness and the discriminative ability of the method, we create kernels of equal size, i.e., K_G, $K_E \in \mathbb{R}^{MxM}$, with $M = k * c$, where c is the number of classes, while k is the number of the most representative samples in each class. For the Euclidean space, we apply a simple k-means algorithm, while for the Grassmannian manifold, we select the most representative Grassmannian points, using as a distance between two points on the manifold, the similarity metric of Eq. (14). To this end, we apply a k-medoids classification approach considering as medoid, the local minimizer of function F:

$$F(m_k) = \frac{1}{n_G}\sum_{i=1}^{n_G} d_G(m_k, g_i) \tag{16}$$

where n_G indicates the total number of Grassmannian points g_i in a medoid m_k and $d_G(\cdot)$ denotes the distance between two Grassmannian points (see Eq. (14)). Having defined the M most representative Grassmannian points among the existing ones, we estimate the Grassmannian kernel matrix as $K_{G\,i,j} = k_G\left(g_i, g_j\right)$, with $i, j = 1, 2, \ldots M$. Similarly, each element of the Euclidean kernel matrix is defined as $K_{E\,i,j} = k_E\left(x_i, x_j\right)$ for each $i, j \in [1, M]$. Subsequently, we estimate the common kernel matrix for the two subspaces as $K_{EG} = K_E^{\circ} K_G$, where $K_{EG} \in \mathbb{R}^{MxM}$ and $\langle\circ\rangle$ is the Handamard product of kernel functions.

Finally, to classify the ECG signals we apply a sparse representation using the following equation according to [32], which enables us to map the input signal y to the Hilbert space of a sparse representation a_s:

$$\min_a \left\|y - a_s C\right\|_2^2 + \lambda\|a_s\|_1 \tag{17}$$

where $y = \Sigma^{1/2}U^T K_{EG}$ and $C = \Sigma^{1/2}U^T$, with $U\Sigma V = K_{EG}$ [33].

For the detection and localization of MI, ECG signals corresponding to myocardial infarction cases were initially discriminated from those of health controls and then they were classified in the following categories: anterior (AMI), antero-lateral (ALMI), antero-septal (ASMI), inferior (IMI) and infero-lateral (ILMI). To this end, each ECG signal represented by a set of sparse coefficients is classified to a class $i = 1 \ldots N$, whose training samples provide the best reconstruction of it. Specifically, the classification is performed by assigning each multi-lead ECG signal x to the class minimizing the following residual:

$$\text{Class(i)} = \arg\min_i \left\|x - \delta_i(a_s)\, C\right\| \tag{18}$$

where δ_i sets to zero the coefficients of a_s that do not correspond to class i. The estimation of the sparse representations of ECG signals is achieved using the SPAMS toolbox of Matlab.

2.4.2. Fusion in a Hilbert space through VLAD encoding

In this second fusion approach, we attempt to apply VLAD encoding on Grassmann manifold, as in the case of the Euclidean space, and then concatenate the two VLAD representations to form a joint representation for the two spaces (it is defined as *proposed-2*). In other words, we use VLAD encoding as a means to map our features into a common space (Fig. 3).

In contrast with the previous approach, in this case, we divide each signal into overlapping equally-sized elementary signals (using a sliding window of a constant size W) that are modeled by a linear dynamical system. In this way, each ECG signal is finally represented as a set of points on the Grassmann manifold instead of a single point. Subsequently, we apply a Karcher mean algorithm [34] to estimate the codewords m_i in Eq. (12). We re-identify the members G_j of each class, i.e., $m_i = NN(G_j)$, using the dissimilarity metric defined in Eq. (14). Hence, the VLAD encoding of an ECG signal on the Grassmann manifold for a codebook of q representative

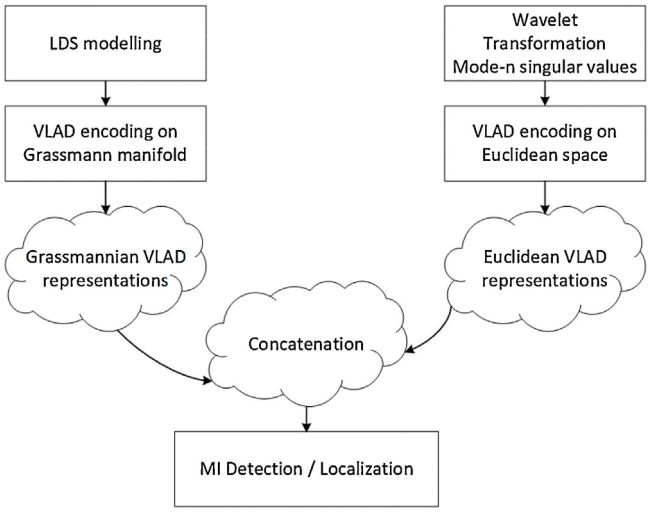

Fig. 3. Proposed-2 fusion approach in a Hilbert space through VLAD encoding.

words, $\left\{m_i\right\}_{i=1}^{q}$, can be defined as:

$$\bar{V}_{Grassmannian} = \frac{\bar{V}}{\left\|\bar{V}\right\|_2} = \frac{1}{\left\|\bar{V}\right\|} \times \left\{ \sum_{\substack{G_j \text{ such that} \\ \text{the Karcer mean} \\ m_1 = NN(G_j)}} \left\|exp_{m_1}^{-1} G_j\right\|_F, \ldots, \sum_{\substack{G_j \text{ such that} \\ \text{the Karcer mean} \\ m_q = NN(G_j)}} \left\|exp_{m_q}^{-1} G_j\right\|_F \right\} \tag{19}$$

For the final classification of an ECG signal to one of the five classes (localization), i.e., anterior (AMI), antero-lateral (ALMI), antero-septal (ASMI), inferior (IMI) and infero-lateral (ILMI), we concatenate the two VLAD encodings, i.e., $\bar{V}_{ECG} = \left[\bar{V}_{Euclidean}\, \bar{V}_{Grassmannian}\right]$, to form a joint feature representation and finally use a simple SVM classifier. We have to note here that when sub-band tensors of wavelet transform are modeled using higher-order linear dynamical systems, the system creates multiple Grassmannian subspaces. In our experiments, we used in total five sub-bands, A_7, D_4, D_5, D_6 and D_7 and therefore in this case the final vector $\bar{V}_{ECG}$ was produced by the concatenation of one Euclidean with six Grassmannian feature representations, i.e., $\bar{V}_{ECG} = \left[\bar{V}_E\, \bar{V}_G\, \bar{V}_G^{A_7}\, \bar{V}_G^{D_4} \ldots \bar{V}_G^{D_7}\right]$.

3. Results

For the evaluation of the proposed method we conducted extensive tests using a publicly available dataset, namely PTB Diagnostic ECG database [35], containing multi-lead ECG data. Each record in the dataset includes 15 simultaneously measured signals, i.e., the conventional 12 leads as shown in Fig. 4 (i, ii, iii, avr, avl, avf, v1, v2, v3, v4, v5, v6) together with the 3 Frank lead ECGs (vx, vy, vz) (in our experiments the 3 Frank lead ECGs were not used, Fig. 4). Fig. 5 shows a 3D representation of a beat period of an ECG signal of the PTB Diagnostic database. Each signal is digitized at 1000 samples per second. More specifically, the dataset contains in total 549 records of 290 subjects from different diagnostic classes: Myocardial infarction (148), Cardiomyopathy/Heart failure (18), Bundle branch block (15), Dysrhythmia (14), Myocardial

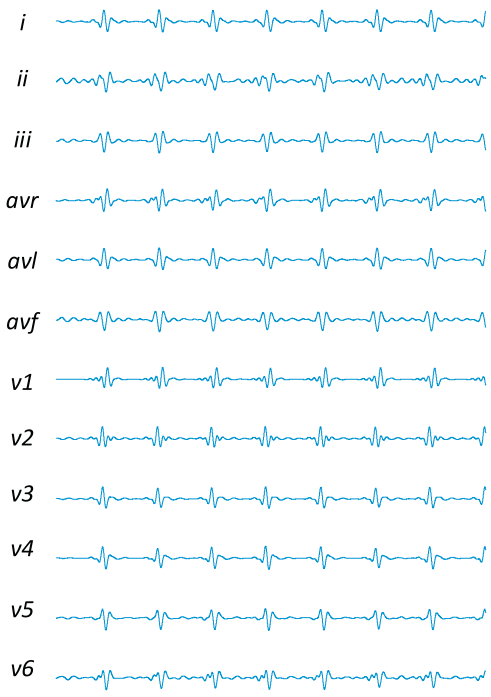

Fig. 4. The 12 leads of an ECG signal of the PTB Diagnostic database.

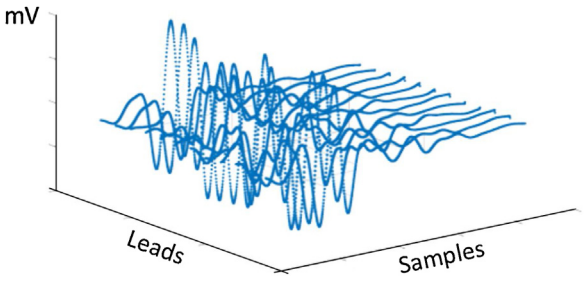

Fig. 5. A beat period of an ECG signal of the PTB Diagnostic database.

hypertrophy (7), Valvular heart disease (6), Myocarditis (4), Miscellaneous (4), Healthy controls (52). In the case of MI patients, the location of the infarction in the myocardium is classified in different categories [36]. Nevertheless, in our experiments five groups of these have been considered (anterior (AMI), antero-lateral (ALMI), antero-septal (ASMI), inferior (IMI) and infero-lateral (ILMI)). The records of these categories are 47 from AMI, 43 from ALMI, 77 from ASMI, 89 from IMI and 56 from ILMI. The other 56 records from MI subjects correspond to other groups of MI location, but these groups have a very limited number of ECG records to be used for training the classifier.

The goal of this experimental evaluation is three-fold. Firstly, we aim to define the optimal parameters for the two proposed fusion approaches. Secondly, a detailed experimental evaluation for the contribution of each extracted feature and fusion approach is performed estimating the MI detection and localization rates. Finally, in order to validate the efficiency of the proposed method, we compared its detection and localization rates with those of various state-of-the-art approaches using the same dataset.

3.1. Estimating the optimal parameters

The first evaluation phase concerns the selection of the optimal parameters for both fusion approaches in order to achieve the best detection rates. Initially, we carried out experiments in order to define the most appropriate kernel function for the mapping of Euclidean data into the Reproducing Kernel Hilbert Space (*proposed-1* approach). In particular, we experimented using three kernel functions, namely radial basis function (RBF), polynomial and exponential chi-square distance. Fig. 6 presents the classification rates for each kernel function when they are applied for the mapping of Euclidean data into a common Hilbert Space. As we can easily see, the best classification rate (100%) is achieved by using the RBF kernel function, while the polynomial and chi-square kernels provide lower detection rates of 99.6% and 93.8%, respectively.

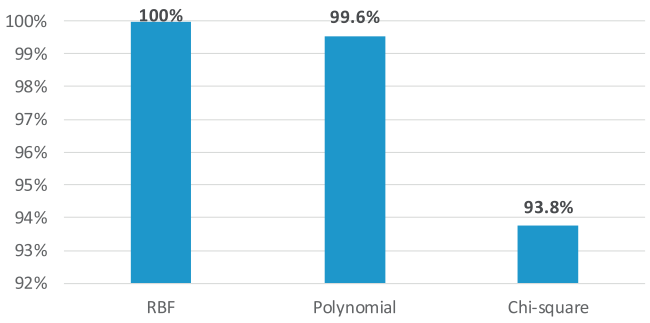

Fig. 6. Detection accuracy rates for proposed-1 fusion approach using different kernel functions for mapping Euclidean data into a common Hilbert space.

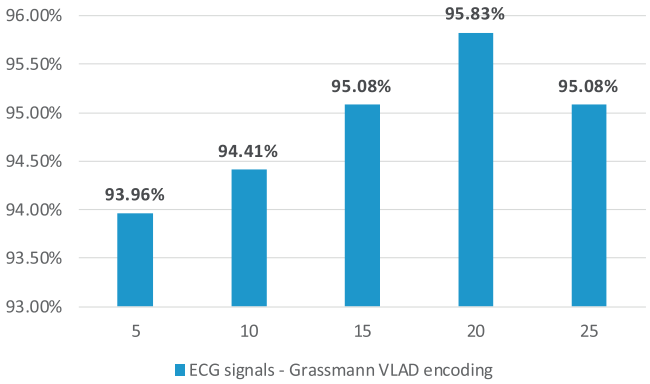

Fig. 7. Detection rates of Grassmann VLAD encoding $\bar{V}_G$ (*proposed-2* approach) using different window sizes W.

On the other hand, for the second fusion approach (*proposed-2*), we attempt to find the most appropriate sliding window size W for dividing the multi-dimensional signal into overlapping equally sized elementary signals. This approach allows us to represent each signal as a set of points on the Grassmann manifold instead of a single point. Towards this end, we carried out experiments using five different window sizes (5, 10, 15, 20 and 25 length) for creating the elementary equally sized signals. As seen in Fig. 7, the best classification rate is achieved by setting the window size equal to 20, yielding a detection rate of 95.83% (this detection rate refers to the VLAD encoding $\bar{V}_G$ and not to the concatenated $\bar{V}_{ECG}$ vector). It is worth mentioning that when small signal sizes are used, the detection rates decrease, apparently due to the lack of sufficient information in each sub-signal, while the detection rate for signal sizes larger than 20 also seems to decrease.

3.2. Contribution of different feature representations to the detection of myocardial infraction

In this subsection, we elaborate a more detailed analysis in order to evaluate the contribution of different feature representations to the MI detection process. Specifically, we analyze the contribution of four different feature representations: a) The representation of ECG signal as a single Grassmann point (*proposed-1* approach).

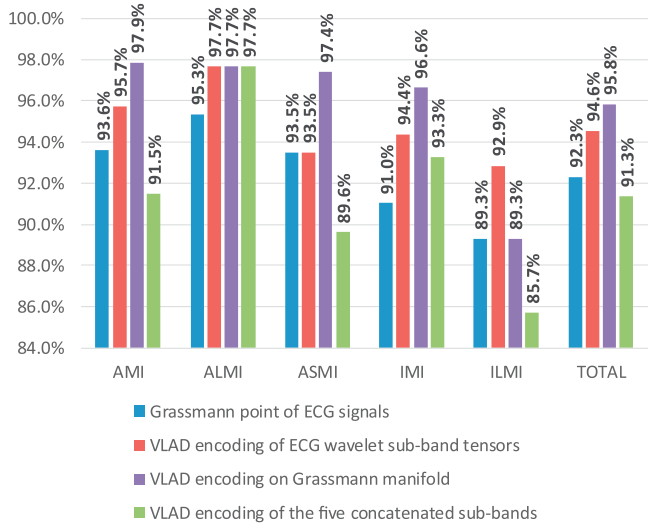

Fig. 8. MI detection rates for the individual feature representations.

b) The VLAD encoding representation $\bar{V}_E$ of the ECG signal after the dyadic discrete wavelet transform and the subsequent multi-scale higher-order SVD analysis on sub-band tensors (*proposed-1* and *proposed-2* approach). c) The VLAD encoding representation on the Grassmann manifold (*proposed-2* approach) using a single Grassmann subspace i.e., $\bar{V}_G$ and d) The concatenated VLAD encoding representation of the five sub-bands, A_7, D_4, D_5, D_6 and D_7 (*proposed-2* approach).

For the classification of the ECG signals, in the first case, i.e., Grassmannian subspace, we used as a similarity metric the distance between two Grassmannian points, as defined in Eq. (14), while in the cases of VLAD encodings we used a standard SVM classifier. The experimental results in Fig. 8 show that VLAD encoding on Grassmann manifold, i.e., $\bar{V}_G$, achieves the best results, with a detection rate of 95.8% against 94.6%, 92.3% and 91.3% for the VLAD encoding representation $\bar{V}_E$, the Grassmann feature representation and the concatenated VLAD vector, respectively. In the next section, we show that by mapping these features to a common Hilbert space, we can further improve the classification accuracy of individual features.

3.3. Comparison of fusion approaches

In this subsection, we aim to evaluate the effect of the two proposed fusion approaches to the detection and localization of MI. In the first approach (*proposed-1*), we use kernel functions to map the Grassmann feature representation and VLAD encoding $\bar{V}_E$ into a common Hilbert space and then apply sparse coding, while for the second approach (*proposed-2*) we create two concatenated VLAD vectors $\bar{V}_{ECG} = \left[\bar{V}_E\, \bar{V}_G\, \bar{V}_G^{A_7}\, \bar{V}_G^{D_4} \ldots \bar{V}_G^{D_7}\right]$ and $\bar{V}_{ECG} = \left[\bar{V}_E\, \bar{V}_G\right]$ and use a standard SVM classifier.

As we can see in Fig. 9, all approaches provide excellent detection rates and can easily distinguish MI cases from those of healthy controls. Additionally, considering the five types of MI, namely AMI, ALMI, ASMI, IMI and ILMI, the localization rates are 100%, 99.7% and 98.4% for *proposed-1*, *proposed-2* with $\bar{V}_{ECG} = \left[\bar{V}_E\, \bar{V}_G\, \bar{V}_G^{A_7}\, \bar{V}_G^{D_4} \ldots \bar{V}_G^{D_7}\right]$ and *proposed-2* with $\bar{V}_{ECG} = \left[\bar{V}_E\, \bar{V}_G\right]$, respectively. It is also worth mentioning that although the feature representation of VLAD encoding $\bar{V}_G$ on Grassmann manifold provides better results than a simple Grassmann feature, the fusion through a Reproducing Kernel Hilbert Space achieves better results in the case of localization. In addition, the accuracy rates of both approaches in Fig. 9 make evident that the individual feature representations contain complementary information and therefore the detection accuracy after fusion is increased.

3.4. Comparison with state-of-the-art approaches

In this last section, we present a comparative analysis of the proposed method against a number of state-of-the-art approaches. More specifically, we compare the Sensitivity, Specificity and Accuracy rates of the proposed method (Table I) against those of ten state-of-the-art approaches that have been used in the past for the detection and localization of MI on PTB Diagnostic ECG database.

To ensure a fair comparison, we adopted the same experimental protocol followed in [19]. The experimental results in Table I show that the proposed method (both proposed-1 and proposed-2 approaches) outperform all other methods achieving improvements up to 0.7% in detection accuracy from [22] and up to 1.9%, 1.3%, 0.4% and 1.2% in localization accuracies from [19,37,18,17], respectively.

4. Discussion

The method of 12-lead simultaneous recording of electrocardiographs allows the capturing of the ECG signal of the same cardiac cycle on 12 leads at the same time. This approach can significantly increase the accuracy of all measurements and reduce the variability of ECG measurement [39]. In a multi-lead ECG, the leads refer to imaginary lines between two ECG electrodes. To exploit this information and better model possible beat and lead correlations, we use a third-order tensor structure and then we attempt to extract different feature representations containing complementary information with regard to the dynamics of ECG signals. This fact justifies the superiority of the proposed method against all other state of the art approaches in Table I. While discrete wavelet transform

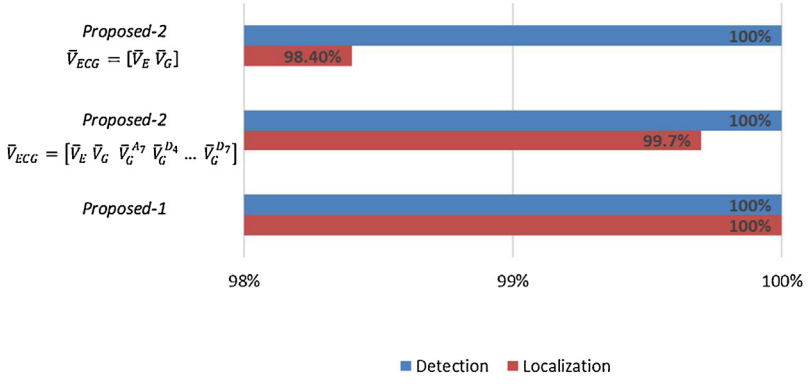

Fig. 9. Detection and localization accuracy rates using the proposed fusion schemes.

Table 1
Detection and localization comparison results.

	Detection			Localization
	Sen	Spe	Acc	Acc
Proposed-1	**100%**	**100%**	**100%**	**100%**
Proposed-2	**100%**	**100%**	**100%**	**99.7%**
Liu et al. [22]	99.8%	97.4%	99.3%	NA
Acharya et al. [5]	95.5%	94.2%	95.2%	NA
Padhy et al. [19]	94.6%	96%	95.3%	98.1%
Sadhukhan et al. [16]	98.2%	97.4%	97.4%	NA
Acharya et al. [37]	99.5%	96.3%	98.8%	98.7%
Sharma et al. [18]	93%	99%	96%	99.6%
Arif et al. [17]	99.97%	99.9%	NA	98.8%
Sun et al. [3]	92.6%	82.4%	NA	76.6%
Jayachandran et al. [15]	NA	NA	95.9%	NA
Nugent et al. [38]	78%	97.3%	NA	NA

has been widely used in the past for modeling ECG signals, it is the first time that linear dynamical systems, and their projection to Grassmann manifold, are used for the modeling of such data. Linear dynamical systems have shown great ability to model dynamical information in video sequences [40], while recently they have been used for the extension of residual networks, i.e., ResNets, and the improvement of Faster-CNN network's accuracy in object detection applications [41]. The experimental results in Fig. 9 show that the combination of LDS descriptors with those extracted from DWT increases significantly the detection rates of individual feature representations presented in Fig. 8.

While both fusion approaches outperform all other state of the art approaches in Table 1, we can notice that the first approach, based on the mapping of both Grassmannian and Euclidean features in a Reproducing Kernel Hilbert Space, provides excellent results in both cases, i.e., detection and localization. In other words, even when the number of classes increases in the case of localization, the discrimination ability of the method remains extremely high, i.e., localization accuracy 100% for *proposed-1* against that of 99.7% for *proposed-2*. This is mainly because in the case of VLAD encoding, we mostly keep a statistical information associated with the spatial distribution of descriptors in the geometrical subspaces, while in the case of mapping of feature representations in a Reproducing Kernel Hilbert Space, we are able to better maintain the dynamics and appearance information of the signals encoded in the descriptors. We have to notice that both approaches proposed in the paper are generic and can be easily applied to other application fields, where the fusion of feature representations that belong to different geometrical subspaces and are extracted from either shallow or deep classifiers is required.

In terms of computational efficiency, both proposed-1 and proposed-2 approaches yield similar results. Specifically, the proposed-1 approach achieves detection and localization of MI in 0.51 s, while the proposed-2 approach achieves classification of an ECG signal in 0.44 s. This difference that is observed between the two approaches is due to the procedure of mapping the data to a Reproducing Kernel Hilbert Space in the proposed-1 approach. Finally, it is worth mentioning that further optimization of the developed algorithms and their computational speed is possible.

5. Conclusions

In this paper, we presented a novel methodology for assisting doctors in detection and localization of MI. The main advantage of the proposed approach is that it exploits better the intercorrelations between signals of different ECG leads by extracting feature representations that lie in different geometrical spaces and contain complementary information with regard to the dynamics of signals. More specifically, we initially reshape the multidimensional signal into a third-order tensor structure and subsequently extract feature representations in both Euclidean and Grassmannian spaces. Moreover, two different methods are proposed for the mapping of two different feature representations into a common Hilbert space before the final classification of signals. The first approach is based on the mapping of both Grassmannian and Euclidean features in a Reproducing Kernel Hilbert Space (RKHS), while the second one attempts to apply VLAD encoding directly to Grassmann manifold and then concatenate the two VLAD representations. The experimental results showed that the proposed method improved significantly the performance of the automated computer-based detection and localization of MI. In the future, more data will be collected in order to assess the effectiveness of the proposed methodology. Finally, we aim to extend and apply the proposed methodology to other application fields, using different types of signals e.g. EEG or EMG, in order to provide a generalized automated electrodiagnostic tool.

Conflict of interest statement

We declare that we have no financial and personal relationships with other people or organizations that can inappropriately influence our work, there is no professional or other personal interest of any nature or kind in any product, service and/or company that could be construed as influencing the position presented in, or the review of, the manuscript entitled, "Multi-lead ECG Signal Analysis for Myocardial Infarction Detection and Localization through the Mapping of Grassmannian and Euclidean Features into a Common Hilbert Space".

Acknowledgement

The research leading to these results has received funding from EC under grant agreement no. H2020-690494 "i-PROGNOSIS".

References

[1] World Health Organization, Cardiovascular Diseases (CVDs), 2018 (Accessed 14 June 2018) http://www.who.int/news-room/fact-sheets/detail/cardiovascular-diseases-(cvds)/.
[2] National Heart, Lung, and Blood Institute, What Is a Heart Attack, 2018 (Accessed 2 July 2018) https://www.nhlbi.nih.gov/health/health-topics/topics/heartattack/.
[3] L. Sun, Y. Lu, K. Yang, S. Li, ECG analysis using multiple instance learning for myocardial infarction detection, IEEE Trans. Biomed. Eng. 59 (12) (2012) 3348–3356, http://dx.doi.org/10.1109/TBME.2012.2213597.
[4] E.J.D.S. Luz, W.R. Schwartz, G. Cámara-Chávez, D. Menotti, ECG-based heartbeat classification for arrhythmia detection: a survey, Comput. Methods Progr. Biomed. 127 (2016) 144–164, http://dx.doi.org/10.1016/j.cmpb.2015.12.008.
[5] U.R. Acharya, H. Fujita, S.L. Oh, Y. Hagiwara, J.H. Tan, M. Adam, Application of deep convolutional neural network for automated detection of myocardial infarction using ECG signals, Inf. Sci. 415 (2017) 190–198, http://dx.doi.org/10.1016/j.ins.2017.06.027.
[6] O. Faust, U.R. Acharya, T. Tamura, Formal design methods for reliable computer-aided diagnosis: a review, IEEE Rev. Biomed. Eng. 5 (2012) 15–28, http://dx.doi.org/10.1109/RBME.2012.2184750.
[7] S. Lahmiri, Comparative study of ECG signal denoising by wavelet thresholding in empirical and variational mode decomposition domains, Healthc. Technol. Lett. 1 (3) (2014) 104–109.
[8] S. Lahmiri, M. Boukadoum, Physiological signal denoising with variational mode decomposition and weighted reconstruction after DWT thresholding, May, 2015 IEEE International Symposium on Circuits and Systems (ISCAS) (2015) 806–809.
[9] S. Lahmiri, M. Boukadoum, A weighted bio-signal denoising approach using empirical mode decomposition, Biomed. Eng. Lett. 5 (2) (2015) 131–139.
[10] S. Padhy, L.N. Sharma, S. Dandapat, Multilead ECG data compression using SVD in multiresolution domain, Biomed. Signal Process. Control 23 (2016) 10–18, http://dx.doi.org/10.1016/j.bspc.2015.06.012.
[11] S. Lahmiri, M. Boukadoum, Hybrid discrete wavelet transform and Gabor filter banks processing for features extraction from biomedical images, J. Med. Eng. 2013 (2013).
[12] D. Giri, U.R. Acharya, R.J. Martis, S.V. Sree, T.C. Lim, T. Ahamed VI, J.S. Suri, Automated diagnosis of coronary artery disease affected patients using LDA, PCA, ICA and discrete wavelet transform, Knowl. Based Syst. 37 (2013) 274–282, http://dx.doi.org/10.1109/RBME.2012.2184750.

[13] M. Kumar, R.B. Pachori, U.R. Acharya, An efficient automated technique for CAD diagnosis using flexible analytic wavelet transform and entropy features extracted from HRV signals, Expert Syst. Appl. 63 (2016) 165–172, http://dx.doi.org/10.1016/j.eswa.2016.06.038.
[14] Q. Zhao, L. Zhang, ECG feature extraction and classification using wavelet transform and support vector machines, Proceedings of the IEEE International Conference on Neural Networks and Brain vol. 2 (2005) 1089–1092, http://dx.doi.org/10.1109/ICNNB.2005.1614807.
[15] E.S. Jayachandran, Analysis of myocardial infarction using discrete wavelet transform, J. Med. Syst. 34 (6) (2010) 985–992, http://dx.doi.org/10.1007/s10916-009-9314-5.
[16] D. Sadhukhan, S. Pal, M. Mitra, Automated ECG analysis using Fourier harmonic phase, Proceedings of the IEEE Region 10 Symposium (TENSYMP) (2017) 1–5, http://dx.doi.org/10.1109/TENCONSpring.2017.8070022.
[17] M. Arif, I.A. Malagore, F.A. Afsar, Detection and localization of myocardial infarction using k-nearest neighbor classifier, J. Med. Syst. 36 (1) (2012) 279–289, http://dx.doi.org/10.1007/s10916-010-9474-3.
[18] L.N. Sharma, R.K. Tripathy, S. Dandapat, Multiscale energy and eigenspace approach to detection and localization of myocardial infarction, IEEE Trans. Biomed. Eng. 62 (7) (2015) 1827–1837, http://dx.doi.org/10.1109/TBME.2015.2405134.
[19] S. Padhy, S. Dandapat, Third-order tensor based analysis of multilead ECG for classification of myocardial infarction, Biomed. Signal Process. Control 31 (2017) 71–78, http://dx.doi.org/10.1016/j.bspc.2016.07.007.
[20] S. Kiranyaz, T. Ince, M. Gabbouj, Real-time patient-specific ECG classification by 1-D convolutional neural networks, IEEE Trans. Biomed. Eng. 63 (3) (2016) 664–675, http://dx.doi.org/10.1109/TBME.2015.2468589.
[21] M. Zubair, J. Kim, C. Yoon, An automated ECG beat classification system using convolutional neural networks, Proceedings of the Sixth IEEE International Conference on IT Convergence and Security (ICITCS) (2016) 1–5, http://dx.doi.org/10.1109/ICITCS.2016.7740310.
[22] N. Liu, L. Wang, Q. Chang, Y. Xing, X. Zhou, A simple and effective method for detecting myocardial infarction based on deep convolutional neural network, J. Med. Imaging Health Inform. 8 (7) (2018) 1508–1512, http://dx.doi.org/10.1166/jmihi.2018.2463.
[23] P. Barmpoutis, K. Dimitropoulos, N. Grammalidis, Smoke detection using spatio-temporal analysis, motion modeling and dynamic texture recognition, September, 2014 22nd European Signal Processing Conference (EUSIPCO) (2014) 1078–1082.
[24] K. Dimitropoulos, P. Barmpoutis, A. Kitsikidis, N. Grammalidis, Classification of multidimensional time-evolving data using histograms of grassmannian points, IEEE Trans. Circuits Syst. Video Technol. 28 (4) (2018) 892–905, http://dx.doi.org/10.1109/TCSVT.2016.2631719.
[25] K. Dimitropoulos, P. Barmpoutis, C. Zioga, A. Kamas, K. Patsiaoura, N. Grammalidis, Grading of invasive breast carcinoma through Grassmannian VLAD encoding, PLoS One 12 (9) (2017) e0185110, http://dx.doi.org/10.1371/journal.pone.0185110.
[26] G. Doretto, A. Chiuso, Y.N. Wu, S. Soatto, Dynamic textures, Int. J. Comput. Vis. 51 (2) (2003) 91–109, http://dx.doi.org/10.1023/A:1021669406132.
[27] K. Dimitropoulos, P. Barmpoutis, N. Grammalidis, Higher order linear dynamical systems for smoke detection in video surveillance applications, IEEE Trans. Circuits Syst. Video Technol. 27 (5) (2017) 1143–1154, http://dx.doi.org/10.1109/TCSVT.2016.2527340.
[28] S.M. Siddiqi, B. Boots, G.J. Gordon, A constraint generation approach to learning stable linear dynamical systems, Adv. Neural Inf. Process. Syst. (2008) 1329–1336.
[29] G. Arfken, Gram-schmidt orthogonalization, Math. Methods Phys. 3 (1985) 516–520.
[30] H. Jégou, M. Douze, C. Schmid, P. Pérez, Aggregating local descriptors into a compact image representation, Proceedings of the IEEE International Conference on Computer Vision and Pattern Recognition (CVPR) (2010) 3304–3311, http://dx.doi.org/10.1109/CVPR.2010.5540039.
[31] V. Kantorov, I. Laptev, Efficient feature extraction, encoding and classification for action recognition, Proceedings of the IEEE International Conference on Computer Vision and Pattern Recognition (CVPR) (2014) 2593–2600, http://dx.doi.org/10.1109/CVPR.2014.332.
[32] A.Y. Wright, A.G. Yang, S.S. Sastry, M. Yi, Robust face recognition via sparse representation, IEEE Trans. Pattern Anal. Mach. Intell. 31 (2) (2009) 210–222, http://dx.doi.org/10.1109/TPAMI.2008.79.
[33] D. Kastaniotis, I. Theodorakopoulos, G. Economou, S. Fotopoulos, Gait based recognition via fusing information from Euclidean and Riemannian manifolds, Pattern Recognit. Lett. 84 (2016) 245–251, http://dx.doi.org/10.1016/j.patrec.2016.10.012.
[34] H. Karcher, Riemannian center of mass and mollifier smoothing, Commun. Pure Appl. Math. 30 (5) (1977) 509–541, http://dx.doi.org/10.1002/cpa.3160300502.
[35] A.L. Goldberger, L.A. Amaral, L. Glass, J.M. Hausdorff, P.C. Ivanov, R.G. Mark, H.E. Stanley, Physiobank, physiotoolkit, and physionet, Circulation 101 (23) (2000) e215–e220.
[36] B. Surawicz, T. Knilans, Chou's Electrocardiography in Clinical Practice E-Book: Adult and Pediatric, Elsevier Health Sciences, 2008.
[37] U.R. Acharya, H. Fujita, M. Adam, O.S. Lih, V.K. Sudarshan, T.J. Hong, J.E.W. Koh, Y. Hagiwara, C.C. Chua, K.C. Poo, T.R. San, Automated characterization and classification of coronary artery disease and myocardial infarction by decomposition of ECG signals: a comparative study, Inf. Sci. 377 (2016) 17–29, http://dx.doi.org/10.1016/j.ins.2016.10.013.
[38] C.D. Nugent, J.A.C. Webb, N.D. Black, Feature and classifier fusion for 12-lead ECG classification, Med. Inform. Internet Med. 25 (3) (2000) 225–235, http://dx.doi.org/10.1080/146392300750019217.
[39] B. Chen, W. Guo, B. Li, R.K. Teng, M. Dai, J. Luo, H. Wang, A Study of deep feature fusion based methods for classifying multi-lead ECG, (2018) arXiv preprint arXiv:1808.01721.
[40] K. Dimitropoulos, P. Barmpoutis, N. Grammalidis, Spatio-temporal flame modeling and dynamic texture analysis for automatic video-based fire detection, IEEE Trans. Circuits Syst. Video Technol. 25 (2) (2015) 339–351, http://dx.doi.org/10.1109/TCSVT.2014.2339592.
[41] A. Dimou, D. Ataloglou, K. Dimitropoulos, F. Alvarez, P. Daras, LDS-inspired residual networks, IEEE Trans. Circuits Syst. Video Technol. (2018), http://dx.doi.org/10.1109/TCSVT.2018.2869680.